Measurement of the neutron capture cross-section of ^{238}U using the neutron activation technique

H. Naik · S. V. Surayanarayana · V. K. Mulik · P. M. Prajapati ·
B. S. Shivashankar · K. C. Jagadeesan · S. V. Thakare · D. Raj · S. C. Sharma ·
P. V. Bhagwat · S. D. Dhole · S. Ganesan · V. N. Bhoraskar · A. Goswami

Abstract The ^{238}U(n, γ)^{239}U reaction cross-section at average neutron energy of 3.7 ± 0.3 MeV from the ^{7}Li(p, n)^{7}Be reaction has been determined using activation and off-line γ-ray spectrometric technique. The ^{238}U(n, γ)^{239}U and ^{238}U(n, 2n)^{237}U reaction cross-sections at average neutron energy of 9.85 ± 0.38 MeV from the same ^{7}Li(p, n)^{7}Be reaction have been also determined using the above technique. The experimentally determined ^{238}U(n, γ)^{239}U and ^{238}U(n, 2n)^{237}U reaction cross-sections were compared with the evaluated data of ENDF/B-VII, JENDL-4.0, JEFF-3.1 and CENDL-3.1. The experimental values were found to be in general agreement with the evaluated value based on ENDF/B-VII, and JENDL-4.0 but not with the JEFF-3.1 and CENDL-3.1. The present data along with literature data in a wide range of neutron energies were interpreted in terms of competition between different reaction channels including fission. The ^{238}U(n, γ)^{239}U and ^{238}U(n, 2n)^{237}U reaction cross-sections were also calculated theoretically using the TALYS 1.2 computer code and were also found to be in agreement experimental data.

Keywords ^{238}U(n, γ)^{239}U and ^{238}U(n, 2n)^{237}U reaction cross-sections · ^{7}Li(p, n)^{7}Be reaction · Average neutron energy · E_n = 3.7 ± 0.3 MeV and 9.85 ± 0.38 MeV · Off-line γ-ray spectrometric technique · TALYS calculation

H. Naik (✉) · A. Goswami
Radiochemistry Division, Bhabha Atomic Research Centre,
Mumbai 400 085, India
e-mail: naikhbarc@yahoo.com

S. V. Surayanarayana · S. C. Sharma · P. V. Bhagwat
Nuclear Physics Division, Bhabha Atomic Research Centre,
Mumbai 400 085, India

V. K. Mulik · S. D. Dhole · V. N. Bhoraskar
Department of Physics, University of Pune, Pune 411 007, India

P. M. Prajapati
Department of Physics, Faculty of Science, The M. S. University
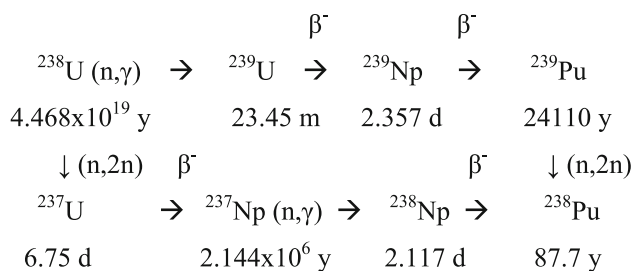of Baroda, Vadodara 390 002, India

B. S. Shivashankar
Department of Statistics, Manipal University,
Manipal 576 104, India

K. C. Jagadeesan · S. V. Thakare
Radiopharmaceutical Division, Bhabha Atomic Research Centre,
Mumbai 400 085, India

D. Raj · S. Ganesan
Reactor Physics Design Division, Bhabha Atomic Research
Centre, Mumbai 400 085, India

Introduction

Most of the reactors operating in the world are light water reactors (PWR and BWR) or heavy water reactors (HWR), which are based on enriched or natural uranium as a fuel. However, recently significant effort has been aimed at generating nuclear power based on the concept of fast reactor [1–5] and advanced heavy water reactor (AHWR) [6–8] to fulfill the increased demand of power production. In AHWR ^{232}Th-^{233}U in the oxide form is used as the primary fuel, whereas in the fast reactor ^{238}U-^{239}Pu in the form of carbide is used as the primary fuel. The ^{239}Pu is first generated in a research reactor from ^{238}U(n, γ)^{239}U reaction and by successive two beta decays. Then the fissile material ^{239}Pu along with ^{238}U is used as a fuel in fast reactor for power generation. The ^{238}U is used as the breeding material to regenerate the fissile material ^{239}Pu. A schematic diagram of the U–Pu fuel cycle is given below.

$$
\begin{array}{ccccccc}
 & & \beta^- & & \beta^- & & \\
^{238}\text{U (n,}\gamma\text{)} & \rightarrow & ^{239}\text{U} & \rightarrow & ^{239}\text{Np} & \rightarrow & ^{239}\text{Pu} \\
4.468\times10^{19}\ \text{y} & & 23.45\ \text{m} & & 2.357\ \text{d} & & 24110\ \text{y} \\
\downarrow \text{(n,2n)} \quad \beta^- & & & & & \beta^- & \downarrow \text{(n,2n)} \\
^{237}\text{U} & \rightarrow & ^{237}\text{Np (n,}\gamma\text{)} & \rightarrow & ^{238}\text{Np} & \rightarrow & ^{238}\text{Pu} \\
6.75\ \text{d} & & 2.144\times10^{6}\ \text{y} & & 2.117\ \text{d} & & 87.7\ \text{y}
\end{array}
$$

In the fast reactor, there is a fast neuron spectrum. Thus for the production of ^{239}Pu, it is necessary to have knowledge about ^{238}U(n, γ)^{239}U and ^{238}U(n, 2n)^{237}U reaction cross-section at various neutron energies. This is because the production of fissile nucleus ^{239}Pu depends on the ^{238}U(n, γ)^{239}U reaction cross-section, which is required with an accuracy of 1–2 % for predicting the dynamical behavior of complex arrangements in fast reactors [9, 10] safely. In fusion-fission hybrid systems, a sensitivity study has shown that the production rate of ^{239}Pu can be predicted within 1 %, provided that the ^{238}U(n, γ)^{239}U cross-section between 3 keV and 3 MeV is known within 2 % [11]. In fast breeder reactors the most important region for neutron capture of ^{238}U lies between 10 and 100 keV [12]. However, in the fast reactor, the neutron energy is on the higher side i.e. from 10 keV to 15 MeV. Above neutron energy of 6.18 MeV the ^{238}U(n, 2n)^{237}U reaction cross-section starts. At neutron energy of 100 keV, the ^{238}U(n, γ)^{239}U reaction cross-section shows a sharp increase trend due to resonance neutron capture. Thereafter it decreases up to 6–7 MeV, where the ^{238}U(n, 2n)^{237}U reaction cross-section starts. The ^{238}U(n, 2n)^{237}U reaction cross-section rapidly increases above threshold energy of 6.18 MeV. Thus, the ^{238}U(n, γ)^{239}U and ^{238}U(n, 2n)^{237}U reaction cross-section at higher neutron energy has a strong impact on the performance and safety assessment for fast reactor [13].

Sufficient ^{238}U(n, γ)^{239}U reaction cross-section data are available in the literature over a wide range of neutron energies from thermal to 18 MeV based on physical measurements [14–24] and activation technique [25–33]. From these data, it can be seen that the ^{238}U(n, γ)^{239}U reaction has numerous resonance cross-section from thermal energy to 0.1 MeV. However, above neutron energy of 0.1 MeV the ^{238}U(n, γ)^{239}U reaction cross-section decreases up to 6–7 MeV [25, 27–29]. Above neutron energy of 7 MeV, the ^{238}U(n, γ)^{239}U reaction cross-section data of D. K. Mc Daniels et al. [23] decreases sharply and remain almost constant up to 14 MeV. At neutron energy of 17 MeV, the ^{238}U(n, γ)^{239}U reaction cross-section data of Panitkin and Tolstikov [27–29] increase sharply and thereafter remain constant up to 20 MeV. So there are three different trends of ^{238}U(n, γ)^{239}U reaction cross-section data within the neutron energy of 0.1–20 MeV [14–29]. In order to examine this aspect, it is important to determine the ^{238}U(n, γ)^{239}U reaction cross-section around these energies regions in spite of the availability of sufficient data in the literature [14–33]. Similar to ^{238}U(n, γ)^{239}U reaction cross-section, sufficient data on ^{238}U(n, 2n)^{237}U reaction cross-section is also available in a wide range of neutron energy above 6 MeV from off-line γ-ray spectrometry and neutron activation methods [34–39]. It can be seen from these data that at neutron energy higher than 6.18 MeV ^{238}U(n, 2n)^{237}U reaction become the pre-dominant mode besides fission and inelastic reaction channels, which are already significant above 1 MeV. The increase of ^{238}U(n, 2n)^{237}U reaction cross-section is very sharp from 6.18 MeV up to the neutron energy of 9.86 MeV and then remains constant up to 13–14 MeV. Thereafter, it decreases with increase of neutron energy due to opening of other channels such as (n, 2nf) and (n, xn) reactions. In view of the above facts, in the present work we have determined the ^{238}U(n, γ)^{239}U reaction cross-section at average neutron energies of 3.7 ± 0.3–9.85 ± 0.38 MeV using the neutron beam from ^{7}Li(p, n) reaction and by activation technique followed by off-line γ-ray spectrometry. The ^{238}U(n, 2n)^{237}U reaction cross-section is also determined at average neutron energy of 9.85 ± 0.38 MeV using the same technique.

Description of the experiment

The experiment was carried out using the 14UD BARC-TIFR Pelletron facility at Mumbai, India [40]. The neutron beam was obtained from the ^{7}Li(p, n)^{7}Be reaction by using the proton beam main line at 6 m height above the analyzing magnet of the Pelletron facility to utilize the maximum proton current from the accelerator. The energy spread for proton at 6 m height above the analyzing magnet was maximum 50–90 keV. At this port, the terminal voltage is regulated by generating voltage mode (GVM) mode using terminal potential stabilizer. The GVM method is commonly used in all particle accelerators to monitor and control the applied voltage. Further, we use a collimator of 6 mm diameter before the target. The lithium foil was made up of natural lithium with thickness of 3.7 mg/cm², sandwiched between two tantalum foils of different thickness. The front tantalum foil facing the proton beam is the thinnest one, with thickness of 3.9 mg/cm², in which degradation of proton energy is only 30 keV. On the other hand the back tantalum foil is the thickest (0.025 mm), which is sufficient to stop the proton beam. Behind the Ta–Li–Ta stack, the samples used for irradiation were placed. The samples consist of natural ^{238}U metal foil and natural indium metal foil, which were wrapped separately with 0.025 mm thick aluminum foil to prevent contamination from one to the other. The size of ^{238}U metal foil was

1.0 cm^2 with thickness of 29.3 mg/cm^2, whereas indium metal foil is also of same size with thickness of 2.6 mg/cm^2. The γ-ray activity of ^{115m}In from ^{115}In(n, n')^{115m}In reaction was used to measure the neutron flux. The isotopic abundance of ^{115}In in natural indium is 95.7 %. The U–In stack was mounted at zero degree with respect to the beam direction at a distance of 2.1 cm from the location of the Ta–Li–Ta stack. A schematic diagram of Ta–Li–Ta stack and U-In stack is given in Fig. 1. Different sets of stacks were made for different irradiations at various neutron energies.

The U-In stacks were irradiated by neutrons for 4–6 h depending upon the energy of proton beam facing the thin tantalum target. The energies of proton beam were 5.6–12 MeV respectively. The proton current during the irradiations varied from 200 nA at 5.6 MeV to 400 nA at 12 MeV and the corresponding maximum neutron energies facing by U-In samples targets were 3.7–10.1 MeV respectively. After irradiation, the samples were cooled for 1 h. Then the irradiated targets of U and In along with Al wrapper were mounted in two different Perspex plates and taken for γ-ray spectrometry. The γ-rays of fission/reaction products from the irradiated U and In samples were counted in an energy and efficiency calibrated 80 c.c. HPGe detector coupled to a PC-based 4 K channel analyzer. The counting dead time was kept always <5 % by placing the irradiated U and In samples at a suitable distance from the detector to avoid pileup effects. The energy and efficiency calibration of the detector system was done by counting the γ-ray energies of standard ^{152}Eu and ^{133}Ba sources [41–46] keeping the same geometry, where the summation error was negligible. The γ-ray energies with their intensities for ^{152}Eu are 121.78 (28.58 %), 244.7 (7.583 %), 344.28 (26.5 %), 367.79 (0.861 %), 411.12 (2.234 %), 443.97 (2.821 %), 688.67 (0.857 %), 867.38 (4.245 %), 964.08 (14.605 %), 1005.27 (0.645 %), 1112.07 (13.644 %), 1212.95 (1.422 %), 1299.14 (1.623 %) and 1408.01 (21.005 %) keV respectively. For ^{133}Ba the γ-ray energies with their intensities are 53.16 (2.199 %), 80.997 (34.06 %), 276.4 (7.164 %), 302.9 (18.33 %), 356.02
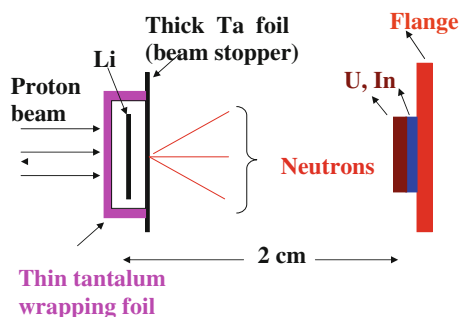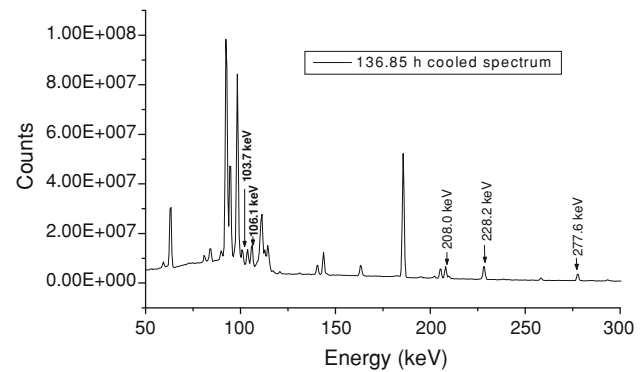
Fig. 2 Gamma ray spectrum of irradiated ^{238}U showing the γ-ray energy of ^{237}U and ^{239}Np

(62.05 %) and 383.85 (8.94 %) keV respectively [41–46]. The standard ^{152}Eu and ^{133}Ba sources were chosen to cover the energy range from 53.16 MeV to 1408.01 keV to avoid so many sources having single or few γ-lines. The γ-ray counting of the standard sources were done at the same geometry keeping in mind the summation error. This was checked by comparing the efficiency obtained from γ-ray counting of standards such as ^{241}Am (59.54 (35.9 %) keV), ^{137}Cs (661.66 (85.1 %) keV), ^{54}Mn (834.55 (99.976 %) keV), ^{60}Co (1173.24 (99.994 %) and 1332.5 (99.986 %) keV) [41–46]. The detector efficiency was 20 % at 1332.5 keV relative to 3″ diameter × 3″ length NaI(Tl) detector. The uncertainty in the efficiency was 2–3 %. The resolution of the detector system had a FWHM of 1.8 at 1332.5 keV of ^{60}Co. The γ-ray counting of the irradiated U and In samples were done alternately in the first day. From second day onwards γ-ray counting of only U sample was done up to few months to check the half-life of the nuclides of interest. A typical 136.85 h cooled γ-ray spectrum of the irradiated ^{238}U sample is given in Fig. 2.

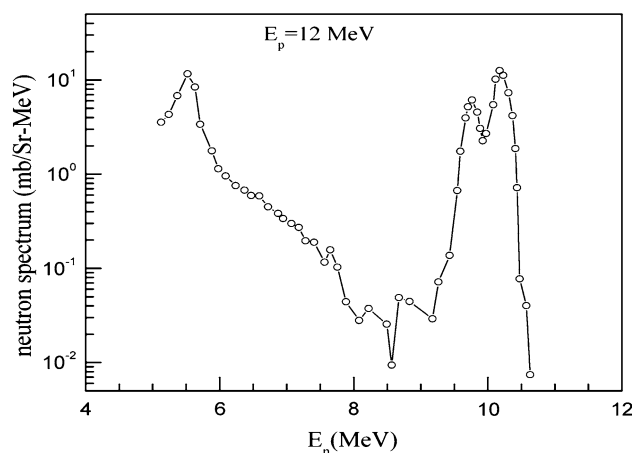## Analysis of the experiment

Calculation of the neutron energy

The incident proton energies in the present experiment were 5.6–12.0 MeV. Degradation of proton energy on the front thin tantalum foil of 3.9 mg/cm^2 thickness is only 30 keV. The Q value for the ^{7}Li(p, n)^{7}Be reaction to the ground state is −1.644 MeV, whereas the first excited state is 0.431 MeV above ground state leading to an average Q value of −1.868 MeV. Thus for the proton energy of 5.6–12.0 MeV the resulting peak energy of first group of neutrons (n$_0$) would be 3.72–10.12 MeV to the ground state of ^{7}Be having threshold 1.881 MeV. Corresponding neutron energy of second group of neutrons (n$_1$), for the first excited state of ^{7}Be will be 3.23–9.63 MeV respectively. This is because

Fig. 1 Schematic diagram showing the arrangement used for neutron irradiation

above proton energy of 2.4 MeV, the n_1 group of neutrons is also produced. Liskien and Paulsen [47] have given the branching ratio to the ground state and first excited state of ^{7}Be up to proton energy of 7 MeV. However, Poppe et al. [48] have given the branching ratio to ground state and first excited state of ^{7}Be for the proton energy of 4.2–26 MeV. In addition to these, Meadows and Smith [49] have also given the branching ratio to the ground state and first excited state ^{7}Be up to 7 MeV. Based on their [47–50] prescription for the proton energy of 5.6 MeV, the contribution to n_0 and n_1 group of neutrons are 86.1–13.9 % respectively. The proton energy of 5.6 MeV leads to average neutron energy of $3.72 \times 0.861 + 3.23 \times 0.139 = 3.651$ MeV. For proton energy of 12 MeV, the contributions to n_0 and n_1 group of neutrons are 60 and 40 % respectively [48]. This leads to average neutron energy of 9.924 MeV.

Above proton energy of 4.5 MeV the fragmentations of the ^{8}Be to ^{4}He + ^{3}He + n ($Q = -3.23$ MeV) occurs and other reaction channels are open to give continuous neutron energy distribution besides n_0 and n_1 groups of neutrons. Meadows and Smith [49] have given experimental neutron distributions from break up channels and also parameterized these distributions. For the proton energy of 5.6 MeV, we have used their parameterization for break up neutrons having a weight of 4 % and two Gaussian distributions with weights of 84 and 12 % for n_0 and n_1 groups of neutron, which is shown in Fig. 3. These Gaussians are centered at 3.7 and 3.2 MeV having a width of 0.3 MeV. For proton energy of 12 MeV, we have extrapolated from the experimental neutron spectrum of Poppe et al. [48] to obtain the neutron spectrum, which is shown in Fig. 4. From Fig. 4, the average neutron energy for (n, γ) and (n, 2n) reactions was obtained as 9.85 ± 0.38 MeV after removing the tailing distribution of the neutron spectrum below 6.5 MeV. This value is slightly lower than the value
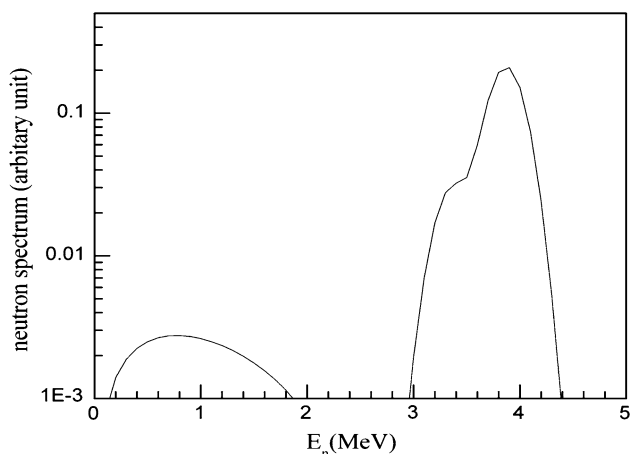
Fig. 4 Extrapolated neutron spectrum in ^{7}Li(p, n) reaction at $E_p = 12$ MeV obtained from neutron spectrum at $E_p = 10$ MeV of Ref. [48]

of 9.924 MeV, which was calculated based on percentage weights of the two groups as mentioned above.

Calculation of the neutron flux

In the present work the neutron beam was obtained from ^{7}Li(p, n)^{7}Be reaction. The proton energy above 4.5 MeV, the fragmentation of ^{8}Be to ^{4}He + ^{3}He + n ($Q = -3.23$ MeV) occurs and other reaction channel opens to give continuous neutron energy distribution besides n_0 and n_1 groups of neutrons. However, the contribution from the second group of neutron is only 13.9 % for the proton energy of 5.6 MeV. Thus, at the neutron energy of 3.7 MeV corresponding to the proton energy of 5.6 MeV, the photo-peak activity of 336.2 keV γ-line of ^{115m}In from ^{115}In(n, n') reaction is used for flux determination. The net area of the full energy photo-peak (A_{net}) for 336.2 keV gamma lines of ^{115m}In was related to the neutron flux (Φ) with the relation.

$$A_{net}(CL/LT) = N\sigma\Phi a\varepsilon (1 - \exp(-\lambda t))\exp(-\lambda T) \\ (1 - \exp(\lambda CL))/\lambda \qquad (1)$$

where N is the number of target atoms and σ is the reaction cross-section of ^{115}In(n, n') ^{115m}In reaction. 'a' is the branching intensity of the 336.2 keV gamma lines of ^{115m}In and ε is its detection efficiency. 't', T, CL and LT are the irradiation time, cooling time, clock time and counting time respectively. In the above equation the CL/LT term has been used for dead time correction.

The net area of the full energy photo-peak (A_{net}) of 336.2 keV γ-lines of ^{115m}In was obtained using PHAST peak fitting program [50]. Taking the cross-section (σ) from literature [51] for ^{115}In(n, n') reaction, neutron flux at average neutron energy of 3.7 MeV was calculated using Eq. (1). The nuclear spectroscopic data such as half-life

Fig. 3 Neutron spectrum from ^{7}Li(p, n) reaction at $E_p = 5.6$ MeV calculated using the results of Meadows and Smith of Ref. [49]

and branching intensity (*a*) were taken from refs. [41–46]. The neuron flux (Φ) at the neutron energy of 3.7 MeV was obtained to be $(8.39 \pm 0.18) \times 10^6$ n cm^{-2} s^{-1}. In the ^{7}Li(p, n)^7 Be reaction, there is a contribution of 13.9 % from second group at neutron energy of 3.23 MeV [53]. Thus the σ values of 13.9 % contribution at 3.23 MeV and 86.1 % at 3.72 MeV were considered for the determination of neutron flux. In order to examine this, the neutron flux was also calculated using the yield (Y) of fission products such as ^{92}Sr or ^{97}Zr, extracted from the experimental yields of Ref. [52] in the 3.7 MeV neutron induced fission of ^{238}U. The equation used for such calculation is as follows.

$$\Phi = \frac{A_{\text{net}}(CL/LT)\,\lambda}{N\sigma_{\text{f}}\text{Ya}\varepsilon\,(1 - \exp(-\lambda t))\exp(-\lambda T)\,(1 - \exp(\lambda CL))} \tag{2}$$

All terms in Eq. (2) have the same meaning as in Eq. (1) except the yield (Y) of the fission product [52, 53] and fission cross-section (σ_{f}), which was taken from Ref. [54].

At average neutron energy of 3.7 MeV, the neutron flux calculated using Eq. (2) is $(9.16 \pm 0.25) \times 10^6$ n cm^{-2} s^{-1}, which is in close agreement with the value $(8.39 \pm 0.18) \times 10^6$ n cm^{-2} s^{-1} obtained from Eq. (1). Folding the neutron spectrum of Fig. 3 [48] with ^{238}U(n, f) cross section [54] at different neutron energies gives average fission cross-section. Using the average ^{238}U(n, f) cross section also gives the similar value of neutron flux. This is due to the negligible tailing in the neutron spectrum for $E_{\text{n}} = 3.7$ MeV corresponding to the proton energy of 5.6 MeV (Fig. 3).

At higher neutron energy, the contribution from the second group and tailing due to break up reaction (^{8}Be → ^{4}He + ^{3}He + n) is more important. It can be also seen from Fig. 4 that in the neutron spectrum from the 12 MeV proton beam, the tailing part of the low energy neutron is quite significant. Within this range of neutron energy, the ^{115}In(n, n')^{115m}In reaction cross-section changes drastically [51]. On the other hand, the neutron induced fission cross-section of ^{238}U [54] and yield of fission products [52, 53] at the peak position of the mass yield curve do not change significantly. In view of this, the neutron flux for (n, γ) reaction at average neutron energy of 9.85 ± 0.38 MeV corresponding proton energy of 12 MeV was calculated using Eq. (2), which is $(1.3 \pm 0.05) \times 10^7$ n cm^{-2} s^{-1}. This higher value of neutron flux at proton energy of 12 MeV is due to higher proton current of 400 nA compared to 100 nA at 5.6 MeV. The neutron flux for (n, 2n) reaction at average neutron energy of 9.85 ± 0.38 MeV corresponding to proton energy of 12 MeV was obtained to be 6.5×10^6 n cm^{-2} s^{-1}. This value was obtained based on the ratio of neutron flux of the neutron spectrum of Fig. 4 for (n, 2n) reactions above its threshold to total flux.

Determination of ^{238}U(n, γ)^{239}U and ^{238}U(n, 2n)^{237}U reaction cross-sections and their results

The nuclear spectroscopic data used in the present work for the calculation of the cross-sections of the ^{238}U(n, γ)^{239}U and ^{238}U(n, 2n)^{237}U reactions, respectively, are taken from the refs. [41, 43–46] and are given in Table 1. The half-life of ^{239}U is 23.54 min., which decays 99.6 % to ^{239}Np within 3 h. In view of this, ^{238}U(n, γ)^{239}U reaction cross-section (σ) can be calculated from the γ-ray activity of ^{239}Np ($T_{1/2} = 2.355$ days) measured after sufficient cooling time making chemical separation unnecessary. Similarly, the ^{238}U(n, 2n)^{237}U reaction cross-section was calculated from the γ-ray activity of ^{237}U obtained from the γ-ray spectrum measured after sufficient cooling time, when ^{239}U could not be detected any more. The net area of the full energy photo-peak (A_{net}) for the γ-lines of ^{237}U and ^{239}Np are obtained by using PHAST [50] fitting program. The equation used for the calculation of cross-sections (σ) of the ^{238}U(n, γ)^{239}U and ^{238}U(n, 2n)^{237}U reactions is given below

$$\sigma = \frac{A_{\text{net}}(CL/LT)\lambda}{N\Phi\text{a}\varepsilon\,(1 - \exp(-\lambda t))\exp(-\lambda T)\,(1 - \exp(\lambda CL))} \tag{3}$$

All terms in Eq. (3) have the similar meaning as in the Eq. (1). The neutron flux (Φ) of $(8.78 \pm 0.38) \times 10^6$ n cm^{-2} s^{-1} was used to calculate the cross-section of the ^{238}U(n, γ)^{239}U reaction at average neutron energy of 3.7 ± 0.3 MeV, which is 15.711 ± 0.986 mb. Similarly, at average neutron energy of 9.85 ± 0.38 MeV the neutron flux (Φ) of $(1.3 \pm 0.05) \times 10^7$ n cm^{-2} s^{-1} was used to calculate the cross-section of the ^{238}U(n, γ)^{239}U reaction, which is 2.242 ± 0.091 mb. On the other hand at average neutron energy of 9.85 ± 0.38 MeV the neutron flux (Φ) of $(6.5 \pm 0.25) \times 10^6$ n cm^{-2} s^{-1} was used to calculate the ^{238}U(n, 2n)^{237}U reaction cross-section, which is 1351 ± 87 mb.

Table 1 Nuclear spectroscopic data used in the calculations was taken from refs. [41–46]

Nuclide	Half life	γ-ray energy (keV)	γ-ray abundance (%)
^{115m}In	4.486 h	336.2	45.9
^{237}U	6.75 days	101.1	26.0
		208.0	22.0
^{239}U	23.54 m	74.7	52.2
^{239}Np	2.355 days	103.7	23.9
		106.1	22.7
		228.2	10.7
		277.9	14.2

For $^{238}U(n, \gamma)^{239}U$ reaction, the low energy neutrons also contribute to the cross-section. It can be seen from Figs. 3 and 4 that the contribution to the neutron flux from the tail region is 4 and 49 % at the proton energy of 5.6–12.0 MeV respectively. In view of this the contribution from the tail region to $^{238}U(n, \gamma)^{239}U$ reaction has been estimated using the ENDF/B-VII [55] and JENDL-4.0 [56] by folding the cross-sections with neutron flux distributions of Figs. 3 and 4. The contribution to the cross-section of the $^{238}U(n, \gamma)^{239}U$ reaction from the above evaluation at E_P = 5.6 MeV are 4.07 and 4.13 mb from ENDF/B-VII [55] and JENDL-4.0 [56], respectively. Similarly, at E_P = 12 MeV, the contribution to the cross-section of the $^{238}U(n, \gamma)^{239}U$ reaction from the above evaluation are 1.02258 and 0.61439 mb from ENDF/B-VII [55] and JENDL-4.0 [56], respectively. The actual value of $^{238}U(n, \gamma)^{239}U$ reaction-cross section due to the neutrons from the main peak of the n_0 and n_1 groups of the neutron spectrum is obtained after subtracting the average cross-section due to neutrons from tail region from the before mentioned experimental data. Thus the actual experimentally obtained $^{238}U(n, \gamma)^{239}U$ reaction cross-sections at average neutron energies of 3.7 ± 0.3 and 9.85 ± 0.38 MeV corresponding to proton energy of 5.6–12 MeV are 11.6 ± 1.0 and 1.42 ± 0.09 mb, which are given in Table 2. Since the neutron spectrum from proton energy of 12 MeV has a tailing (Fig. 4), it contribute about 40 mb to the total $^{238}U(n, 2n)^{237}U$ reaction cross-section. Thus the actual experimentally obtained $^{238}U(n, 2n)^{237}U$ reaction cross-section at average neutron energy of 9.85 ± 0.38 MeV corresponding to proton energy of 12 MeV from present work is 1311 ± 87 mb, which is given in Table 2.

The uncertainties associated to the measured cross-sections come from the combination of two experimental data sets. This overall uncertainty is the quadratic sum of both statistical and systematic errors. The random error in the observed activity is primarily due to counting statistics, which is estimated to be 10–15 %. This can be determined by accumulating the data for an optimum time period that depends on the half-life of nuclides of interest. The systematic errors are due to uncertainties in neutron flux estimation (∼4 %), the irradiation time (∼2 %), the detection efficiency calibration (∼3 %), the half-life of the fission products and the γ-ray abundances (∼2 %) as reported in the literature [41–46]. Thus the total systematic error is about ∼6 %. The overall uncertainty is found to range between 12–17 %, coming from the combination of a statistical error of 10–15 % and a systematic error of 6 %.

Discussion

The $^{238}U(n, \gamma)^{239}U$ reaction cross-section at average neutron energies of 3.7 ± 0.3 and 9.85 ± 0.38 MeV as well as $^{238}U(n, 2n)^{237}U$ reaction cross-section at 9.85 ± 0.38 MeV from present work (Table 2) are the values determined from a different approach than the existing conventional activation technique [25–33]. In the present work the average neutron energies of 3.7 ± 0.3 and 9.85 ± 0.38 MeV were obtained from $^7Li(p, n)$ reaction at proton energies of 5.6 and 12 MeV, respectively. Thus the neutron spectrum has some tailing, which were shown in Figs. 3 and 4. In spite of this, the $^{238}U(n, \gamma)^{239}U$ and the $^{238}U(n, 2n)^{237}U$ reaction cross-sections were extracted at the above neutron energies after correcting the cross-section due to the tail part of the neutron spectrum. Similar approach was also followed in our earlier work [40] for the measurement of neutron induced reaction cross-section of ^{232}Th. Thus the approach used in the present work, for determining the $^{238}U(n, \gamma)^{239}U$ and the $^{238}U(n, 2n)^{237}U$ reaction cross-sections at higher energy neutron is for the first time and different from the conventional methods with mono-energetic neutrons [14–39]. In order to examine this, the experimentally determined $^{238}U(n, \gamma)^{239}U$ and the $^{238}U(n, 2n)^{237}U$ reaction cross-sections from present work were compared with the existing literature data [14–39] based on mono-energetic neutrons. They were found to be in good agreement, which shows the validity of present approach. Further, the experimentally determined $^{238}U(n, \gamma)^{239}U$ and $^{238}U(n, 2n)^{237}U$ reaction cross-sections from the present work were also compared with the evaluated data

Table 2 $^{238}U(n, \gamma)^{239}U$ and $^{238}U(n, 2n)^{237}U$ reaction cross-sections at different neutron energies

Neutron energy (MeV)	Neutron flux (n cm^{-2} s^{-1})	Cross-section (mb)		
		Expt.	ENDF/B-VII	JENDL-4.0
		$^{238}U(n, \gamma)^{239}U$		
3.7 ± 0.3	(8.78 ± 0.38) × 10^6	11.6 ± 1.0	11.7–9.45[a]	10.14–5.4[a]
9.85 ± 0.38	(1.30 ± 0.05) × 10^7	1.42 ± 0.09	1.05–1.24[b]	1.15–1.00[b]
		$^{238}U(n, 2n)^{237}U$		
9.85 ± 0.38	(6.5 ± 0.25) × 10^6	1311 ± 87	1317–1416[c]	1303–1419[c]

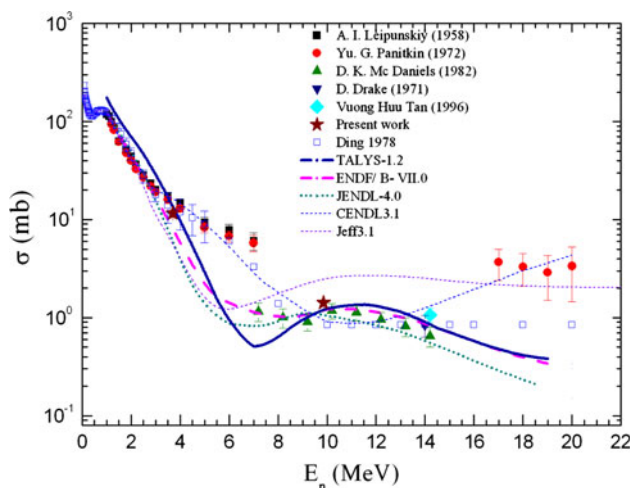For $^{238}U(n, \gamma)^{239}U$ reaction the neutron energy ranges are [a] 3.3–3.8 and [b] 9.0–10.5 MeV

For $^{238}U(n, 2n)^{237}U$ reaction the neutron energy ranges are [c] 9.0–10.5 MeV

from ENDF/B-VII [55], JENDL 4.0 [56], JEFF-3.1 [57] and CENDL-3.1 [58]. These evaluated reaction cross-sections for ^{238}U(n, γ)^{239}U reaction from ENDF/B-VII [55] and JENDL 4.0 [56] are quoted in Table 2 within the neutron energy range of 3.3–3.8 and 9.0–10.5 MeV because of the finite width of neutron energy under the main peak of Figs. 3 and 4. Similarly for the ^{238}U(n, 2n)^{237}U reaction, the evaluated cross-sections from ENDF/B-VII [55] and JENDL 4.0 [56] in Table 2 are quoted within the neutron energy of 9.0–10.5 MeV.

It can be seen from the Table 2 that the present experimental ^{238}U(n, γ)^{239}U and ^{238}U(n, 2n)^{237}U reaction cross-sections are within the range of evaluated data of ENDF/B-VII and JENDL 4.0. However, the evaluated value from JEFF-3.1 and CENDL-3 are not in agreement with the present experimental value and thus are not quoted in Table 2. In order to examine this aspect, the ^{238}U(n, γ)^{239}U reaction cross-sections from the present work and similar data from literature [14–33] given in EXFOR [59] are plotted in Fig. 5. It can be seen from Fig. 5 that the ^{238}U(n, γ)^{239}U reaction cross-section from present work at 3.7 ± 0.3 MeV is in agreement with the value at 3.5–4 MeV of Leipunskiy et al. [25] and Patikin et al. [27]. Similarly, the ^{238}U(n, γ)^{239}U reaction cross-section from present work at 9.85 ± 0.38 MeV is in agreement with the value of Mc Daniels et al. [23]. Further, it can be seen from Fig. 5 that the ^{238}U(n, γ)^{239}U reaction cross-section decreases from 100 keV to 7 MeV. At neutron energy of 7 MeV, the data of Mc Daniels et al. [23] is suddenly lower compared to the data of Leipunskiy et al. [25] and Patikin et al. [27]. Within the neutron energy

Fig. 5 Plot of experimental and evaluated ^{238}U(n, γ)^{239}U reaction cross-section as a function of neutron energy from 1 keV to 20 MeV. Experimental values from present work and from refs. [14–33] are in different symbols, whereas the evaluated and theoretical values from TALYS are in *solid line* of different colors

of 7 up to 15 MeV, the data of Mc Daniels et al. [23] remains nearly constant. At neutron energy of 17 MeV, the data of Patikin et al. [27] suddenly increases and then remains constant up to 20 MeV. In order to examine this, the evaluated data from ENDF/B-VII [55], JENDL-4.0 [56], JEFF-3.1 [57], CENDL [58] and INDC (VN)-8 [60] were plotted in Fig. 5. Similarly, the data based on activation technique from the review article of Ding et al. [61] were also plotted in Fig. 5. It can be seen from Fig. 5 that the evaluated data of CENDL [58] are in agreement with the earlier data from literature [14–33] but not with the present experimental data. The evaluated data of JEF-3.1 [57] shows agreement with the experimental data at lower and higher energy only but not with the data at 3–15 MeV. However, the trend of evaluated data from JEF-3.1 [57] and CENDL [58] is entirely different than the evaluated data from ENDF/B-VII [55], JENDL-4.0 [56]. Similarly, the data of Ding et al. [61] shows agreement with the experimental data evaluated data from ENDF/B-VII [55], JENDL-4.0 [56] at lower energy only but not at higher energy. The experimental data of present work at 3.7 ± 0.3 and 9.85 ± 0.38 MeV as well as the data of McDaniels et al. [23] at 7–15 MeV are in good agreement with the evaluated data of ENDF-B-VII [55] and JENDL [56]. The experimental data of Leipunskiy et al. [25] and Patikin et al. [27] also shows a good agreement with the evaluated data [55, 56] within neutron energy of 1–4 MeV. However, the experimental data of Patkin et al. [28] and Leipunskiy et al. [25] at neutron energy of 5–7 MeV and of Patkin et al. [28] at 17–20 MeV are higher then the evaluated data [55, 56]. To examine this aspect, the ^{238}U(n, γ)^{239}U reaction cross-section at different neutron energy beyond 1 keV was also calculated theoretically using computer code TALYS of version 1.2 [62].

TALYS [62] can be used to calculate the reaction cross-section based on physics models and parameterizations. It calculates nuclear reactions involving targets with mass >12 amu and projectiles like photon, neutron, proton, ^{2}H, ^{3}H, ^{3}He and alpha particles in the energy range of 1 keV–200 MeV. In the present work, we have used neutron energies from 1 keV to 20 MeV for ^{238}U target as done in our earlier work for ^{232}Th [40]. In TALYS, several options are included for the choice of different parameters such as γ-strength functions, nuclear level densities and nuclear model parameters etc. However, we used the default option of various input parameters. Cross-section for all possible outgoing channels for a given projectile (neutron) energy were considered including inelastic and fission channels. However, the cross-sections for the (n, γ) reaction was specially looked for and collected. Theoretically calculated ^{238}U(n, γ)^{239}U reaction cross-section from the neutron energy of 100 keV to 20 MeV using TALYS version 1.2 are also plotted in the Fig. 5.

It can be seen from Fig. 5 that trend of evaluated ^{238}U(n, γ)^{239}U reaction cross-section [55–59] is well reproduced by TALYS 1.2 computer code [62]. However, the theoretical ^{238}U(n, γ)^{239}U reaction cross-section from TALYS are slightly higher than the experimental and evaluated values for neutron energy from 1 keV to 3 MeV. This disagreement is because in TALYS the fission cross-section as a function of neutron energy is quantitatively not well accounted, though the trend is reproduced. However, the values from TALYS are in close agreement with the value of our present work at 3.7–9.85 MeV as well as with the values of McDaniels et al. [23] at 7–15 MeV. On the other hand, the experimental values of Panitkin et al. [28] and Leipunskiy et al. [25] at neutron energy of 5–7 MeV and of Panitkin et al. [28] at 17–20 MeV are higher than the theoretical value of TALYS code [62]. Higher value at 5–7 and 17–20 MeV may be due to the contribution from the low energy neutron. This is because the experiment carried out by them [25, 28] is based on either D + D or D + T reactions, in which the scatted neutron of lower energy must have contributed the higher cross-section. Similar thing was observed in the present work due to lower energy neutron tailing from ^{7}Li(p, n) reaction. Thus the contribution in the ^{238}U(n, γ)^{239}U reaction cross-section due to the low energy neutrons has been corrected in the present work, which has been mentioned earlier in the calculation.

Further, it can be seen from Fig. 5 that the experimental [14–33], evaluated [55–58] and the theoretical [62] ^{238}U(n, γ)^{239}U reaction cross-section decreases from 100 keV to 7 MeV and predict a dip in around 6–8 MeV. Beyond 8 MeV, it increases up to neutron energy of 14 MeV and then again decreases. The dip in the ^{238}U(n, γ)^{239}U reaction cross-section around neutron energy of 6–8 MeV indicates the opening of (n, 2n) reaction channel besides (n, nf) channel. In view of this ^{238}U(n, 2n)^{237}U reaction cross-section from the present work and from literature [34–39] given in EXFOR [59] were plotted in Fig. 6 along with the evaluated data [55, 56]. The ^{238}U(n, 2n)^{237}U reaction cross-sections at different neutron energy was also calculated theoretically using computer code TALYS of version 1.2 [62] and plotted in Fig. 6. It can be seen from Fig. 6 that the ^{238}U(n, 2n)^{237}U reaction cross-section from TALYS shows a close agreement with the experimental data within neutron energy of 8 MeV. Above 8 MeV, the values from TALYS are slightly higher than the experimental data. It can be also seen from Fig. 6 that the experimental and theoretical ^{238}U(n, 2n)^{237}U reaction cross-section shows a sharp increasing trend from the neutron energy of 6.18 to 8 MeV and there after remains constant up to 14 MeV. Thus the increasing trend of ^{238}U(n, γ)^{239}U reaction cross-section beyond 8 up to 14 MeV (Fig. 5) is due to constant ^{238}U(n, 2n)^{237}U reaction cross-section (Fig. 6). It can be also seen from Figs. 5 and 6 that the ^{238}U(n, γ)^{239}U
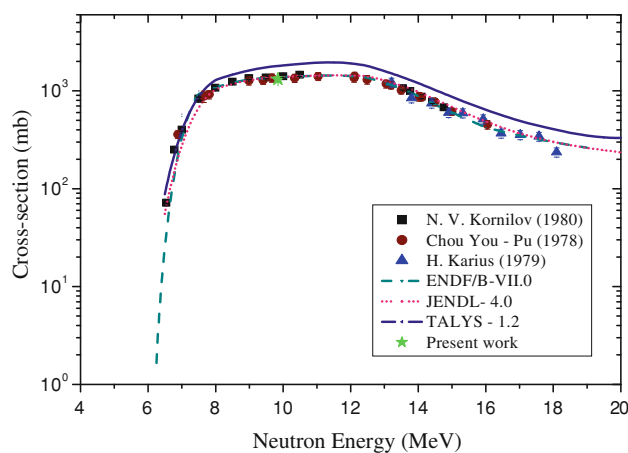
Fig. 6 Plot of experimental and evaluated ^{238}U(n, 2n)^{237}U reaction cross-section as a function of neutron energy from neutron energy 5–20 MeV. Experimental values from present work and from refs. [34–39] are in different symbols, whereas the evaluated and theoretical values from TALYS are in *solid lines* with different colors

reaction cross-section shows a dip, where the ^{238}U(n, 2n)^{237}U and ^{238}U(n, nf) reaction cross-sections show a sharp increasing trend. This is most probably due to the sharing of the excitation energy between ^{238}U(n, γ)^{239}U, ^{238}U(n, 2n)^{237}U and ^{238}U(n, nf) reaction channels in the neutron energy range below 14 MeV. Above the neutron energy of 14 MeV, both ^{238}U(n, γ)^{239}U and ^{238}U(n, 2n)^{237}U reaction cross-sections show a decreasing trend due to opening of (n, 3n) and (n, 2nf) reaction channels.

Conclusions

(i) The ^{238}U(n, γ)^{239}U reaction cross-section at average neutron energies of 3.7 ± 0.3 and 9.85 ± 0.38 MeV as well as the ^{238}U(n, 2n)^{237}U reaction cross-section at 9.85 ± 0.38 MeV are determined using a neutron source from ^{7}Li(p, n) reaction. This is altogether different approach than any conventional technique using mono-energetic neutron source.

(ii) The ^{238}U(n, γ)^{239}U reaction cross-section at average neutron energy 3.7 ± 0.3 and 9.85 ± 0.38 MeV and the ^{238}U(n, 2n)^{237}U reaction cross-section at 9.85 ± 0.38 MeV are in good agreement with the experimental data from literature and the evaluated data from ENDF/B-VII and JENDL-4.0 but not with the evaluated data from CENDL-3 and JEFF-3.1.

(iii) The ^{238}U(n, γ)^{239}U reaction cross-section decreases from neutron energy of 100 keV to 14 MeV with a dip at 6–8 MeV. The ^{238}U(n, 2n)^{237}U reaction increases sharply in the energy range from 6.18 to 8.0 MeV and thereafter it remains constant up to the neutron energy of 14 MeV. Beyond neutron energy of 14 MeV both ^{238}U(n, γ)^{239}U and ^{238}U(n, 2n)^{237}U

reaction cross-sections show decreasing trend due to opening of (n, 3n) and (n, 2nf) reaction channels.

(iv) The ^{238}U(n, γ)^{239}U and ^{238}U(n, 2n)^{237}U reaction cross-sections were calculated theoretically using TALYS code. The theoretical ^{238}U(n, γ)^{239}U reaction cross-section from TALYS are higher than the experimental values within the neutron energy of 1 keV–3 MeV and there after it is agreement with the experimental data. However, the ^{238}U(n, 2n)^{237}U reaction cross-sections from TALYS within neutron energies of 6.18–8 MeV are in good agreement with the experimental data. Above 8 MeV, the values from TALYS are slightly higher than the experimental data.

References

1. Fast Reactors and Accelerator Driven Systems Knowledge Base, IAEA-TECDOC-1319: Thorium fuel utilization: Options and Trends
2. MacDonald PE, Todreas N (2000) Annual Project Status Report 2000, MIT-ANP-PR-071, INEFL/EXT-2009-00994
3. Mathieu L et al (2005) Proportion for a very simple thorium molten salt reactor. In: Proceedings of Global International Conference, Paper No 428, Tsukuba
4. Nuttin A, Heuer D, Billebaud A, Brissot R, Le Brun C, Liatard E, Loiseaux JM, Mathieu L, Meplan O, Merle-Lucotte E, Nifenecker H, Perdu F, David S (2005) Proc Nucl Energy 46:77
5. Allen TR, Crawford DC (2007) Science and Technology of Nuclear Installations, Article ID 97486
6. Sinha RK, Kakodkar A (2006) Design and development of AHWR: the Indian thorium fueled innovative reactor. Nucl Eng Des 236(7–8):683
7. Ganesan S (2006) Creation of Indian experimental benchmarks for thorium fuel cycle, IAEA Coordinated research project on "Evaluated data for thorium–uranium fuel cycle," Third research coordination meeting, 30 Jan–2 Feb 2006, Vienna, INDC (NDS)-0494
8. Ganesan S (2006) Third research co-ordination meeting, Vienna, Austria, INDC (NDS)-0494
9. Pronyaev VG (1999) Summary Report of the Consultants' Meeting on Assessment of Nuclear Data Needs for Thorium and Other Advanced Cycles. INDC (NDS)-408, International Atomic Energy Agency
10. Kuz'minov BD, Manokhin VN (1997) Status of nuclear data for thorium fuel cycle. Nucl Constants 3–4:41
11. Cheng ET, Mathews DR (1979) The influence of nuclear data uncertainties on thorium fusion–fission hybrid blanket nucleonic performance. In: Proceedings of international conference of nuclear cross sections for technology, Knoxville, Tennessee, October 22–26, 1979, p 834, NBS-SP 594, National Bureau of Standards
12. Bartine DE (1979) The use of thorium in fast breeder reactors. In: Proceedings of international conference of nuclear cross sections for technology, Knoxville, Tennessee, October 22–26, 1979, p 119, NBS-SP 594, National Bureau of Standards
13. Pelloni S, Youinou G, Wydler P (1997) Impact of different nuclear data on the performance of fast spectrum based on the thorium–uranium fuel cycle. In: Proceedings of international conference of nuclear data for science and technology, Trieste, May 19–24, 1997, part II, p 1172
14. Batchelor R, Gilboy WB, Jowle JH (1965) Nucl Phys 65:236
15. Asghar M, Chaffey CM, Moxon MC (1966) Nucl Phys 85:305
16. Menlok HO, Poenitz WP (1968) Nucl Sci Eng 33:24
17. Drake D, Bergqvist I, McDaniels DK (1971) Phys Lett B 36:557–559
18. Saussure GD, Silver EG, Perez RB, Ingle R, Weaver H (1973) Nucl Sci Eng 51:385
19. Poenitz WP (1975) Nucl Sci Eng 57:300
20. Liou HL, Chrien RE (1977) Nucl Sci Eng 62:463
21. Wisshak K, Kappeler F (1978) Nucl Sci Eng 66:363
22. Perez RB, de Saussure G, Macklin RL, Halperin J (1979) Phys Rev C 20:528
23. Mc Daniels DK, Varghese P, Drake DM, Arthur F, Lindholm A, Berquist I, Krumlinde J (1982) Nucl Phys A 384:88
24. Voignier J, Joly S, Grenier G (1992) Nucl Sci Eng 112:87
25. Leipunskiy AI, Kazachkovskiy OD, Artyukhov GJa, Baryshnikov AI, Belanova TS, Galkov VI, Stavisskiy YuJa, Stumbur EA, Sherman LE (1958) 58GENEVA 15:50
26. Hann RC, Rose B (1959) J Nucl Eng 8:197
27. Panitkin YuG, Tolstikov VA (1972) Atomnaya Energia 33:782
28. Panitkin YuG, Tolstikov VA (1972) Atomnaya Energia 33:825
29. Panitkin YuG, Tolstikov VA (1975) Atomnaya Energia 39:17
30. Lindner M, Nagle RJ, Landrum JH (1976) Nucl Sci Eng 59:381
31. Poenitz WP, Fawcell LR Jr, Smith DL (1981) Nucl Sci Eng 78:329
32. Buleeva NN, Davletshin AN, Tipunkov OA, Tikhonov SV, Tolstokov VA (1988) Atomnaya Energia 65:348
33. Quang E, Knoll GF (1991) Nucl Sci Eng 110:282
34. Landrum JH, Nagle RJ, Lindner M (1973) Phys Rev C 8:1938
35. Kaius H, Ackermann A, Scobel W (1979) J Phys G 5:715
36. Frchaut J, Bertin A, Bois R (1980) Nucl Sci Eng 74:29
37. Kornilov NV, Zhuravlev BV, Sal'nikov OA, Raich P, Nad' Sh, Darotsi Sh, Sailer K, Chikai I (1980) Atomnaya Energia 49:283
38. Shani G (1983) Ann Nucl Energy 10:473
39. Wang X, Jiang S, He M, Dong K, Xiao C (2010) Nucl Instrum Methods Phys Res A 621:326
40. Naik H, Prajapati PM, Surayanarayana SV, Jagadeesan KC, Thakare SV, Raj D, Mulik VK, Sivashankar BS, Nayak BK, Sharma SC, Mukherjee S, Singh S, Goswami A, Ganesan S, Manchanda VK (2011) Eur Phys J A 47:51
41. Browne E, Firestone RB (1986) Table of Radioactive Isotopes, Shirley VS (ed), Wiley, New York
42. Browne E (2001) Nuclear Data Sheets 93:763
43. Firestone RB, Ekstrom LP (2004) Table of radioactive isotopes, (2004)
44. Blachot J, Fiche Ch (1981) Table of Radioactive Isotopes and their main decay characteristics. Ann Phys 6(1981):3–218
45. Blachot J (2005) Nucl Data Sheets 104:967–1110
46. Singh B, Tuli JK (2005) Nucl Data Sheets 105:109–222
47. Liskien H, Paulsen A (1975) Neutron production cross sections and energies for the reactions ^{7}Li(p, n)^{7}Be and ^{7}Li(p, n)^{7}Be*. At Data Nucl Data Tables 15:57
48. Poppe CH, Anderson JD, Davis JC, Grimes SM, Wong C (1976) Phys Rev C 14:438

49. Meadows JW, Smith DL (1972) Neutrons from proton bombardment of natural lithium, Argonne National Laboratory Report ANL-7983
50. Mukhopadhyaya PK (2001) Personal Communication
51. The international Reactor Dosimetry File:IRDF (2002) Nuclear Data Section, International Atomic Energy Agency
52. Nagy S, Flynn KF, Gindler JE, Meadows JW, Glendenin LE (1978) Phys Rev C 17:163
53. Chapman TC, Anzelon GA, Spitale GC, Nethaway DR (1978) Phys Rev C 17:1089
54. Blons J, Mazur C, Paya D (1975) Phys Rev Lett 35:1749
55. Chadwick MB et al (2006) ENDF/B-VII.0: next generation evaluated nuclear data library for nuclear science and technology. Nucl Data Sheets 107:2931–3060

56. Shibata K et al (2011) JENDL-4.0: a new library for nuclear science and engineering. Nucl Sci Tech 48(1):1
57. Koning AJ, et al (2007) The JEFF evaluated data project. In: Proceeding of the International Conference on Nuclear Data for Science and Technology, Nice
58. China Evaluated Nuclear Data Library CENDL-3.1, (2009)
59. IAEA-EXFOR Database, at http://www-nds.iaea.org/exfor
60. Tan V, Canh Hai N, Trong Hiep N, (1996) INDC (VN)-8
61. Ding D-Z, Guo T-C (1978) HSJ-77106, Review of U-238 capture cross-sections-En = 1 keV to 20 MeV
62. Koning AJ, Hilaire S, Duijvestijn MC (2005) In: Haight RC, Chadwick MB, Kawano T, Talou P (ed) Proceeding of the International Conference on Nuclear Data for Science and Technology-ND 2004, AIP, vol 769. Santa Fe, p 1154